© 2019. Published by The Company of Biologists Ltd | Journal of Cell Science (2019) 132, jcs220871. doi:10.1242/jcs.220871

RESEARCH ARTICLE

EGCG protects cardiomyocytes against hypoxia-reperfusion injury through inhibition of OMA1 activation

Jinliang Nan[2,*], Cunjin Nan[3,*], Jian Ye[2], Lu Qian[1], Ya Geng[4], Dawei Xing[1], Muhammad Saif Ur Rahman[5,‡] and Mingyuan Huang[1,‡]

ABSTRACT

Mitochondria are important for energy production and cardiomyocyte homeostasis. OMA1, a metalloendopeptidase, initiates the proteolytic process of the fusion-allowing protein OPA1, to deteriorate mitochondrial structure and function. In this study, mouse embryonic fibroblasts (MEFs) and neonatal mouse cardiomyocytes (NMCMs) subjected to hypoxia-reperfusion injury (HRI) and/or H_2O_2 were used to mimic oxidative stress in the heart following ischemia-reperfusion injury (IRI). *In vitro* experiments demonstrated that HRI or stimulation with H_2O_2 induced self-cleavage of OMA1 and the subsequent conversion of OPA1 from its long form to its short form, leading to mitochondrial fragmentation, cytochrome c release and apoptosis. By using Molecular Operating Environment (MOE) software to simulate the binding interaction of 2295 phytochemicals against OMA1, epigallocatechin gallate (EGCG) and betanin were selected as candidates of OMA1 inhibitor. We found that EGCG directly interacted with OMA1 and potently inhibited self-cleavage of OMA1, leading to attenuated OPA1 cleavage. This study, therefore, suggests to use OMA1 inhibition induced by EGCG to treat cardiac IRI.

KEY WORDS: Mitochondrial dynamics, EGCG, OMA1, OPA1, Ischemia-reperfusion injury

INTRODUCTION

Mitochondria are the main energy-producing organelles in mammalian cells. In addition to their roles in oxidative metabolism, mitochondria play crucial roles in the pathophysiological processes of cardiomyocytes (Lemieux and Hoppel, 2009). It has been well established that mitochondria are closely associated with the progression of cardiomyopathy in response to various stresses, such as ischemia-reperfusion injury (IRI), hyperglycemia and pressure overload (Biala and Kirshenbaum, 2014; Neuzil et al., 2007).

Mitochondria are dynamic organelles that continuously fluctuate between fission and fusion events, which is referred to as mitochondrial dynamics (Nan et al., 2017). Recently, studies have suggested that mitochondrial dynamics are crucial for the regulation of mitochondrial metabolism in order to meet adequate metabolic demands of the heart and, eventually, protect cardiomyocytes from apoptotic stimuli (Nan et al., 2017; Wai and Langer, 2016). Abnormalities in mitochondrial dynamics contribute to the pathogenesis of the heart (Dorn, 2015).

Mitochondrial dynamics are mainly operated by mitochondrial fission and fusion proteins, i.e. mitochondrial dynamics-related proteins most of which are dynamin-like proteins that contain a GTPase domain (Dorn, 2015). These proteins are located in the outer mitochondrial membrane (OMM), intermembrane space (IMS) or inner mitochondrial membrane (IMM) (Cogliati et al., 2013). Dynamin-related protein1 (Drp1) is mainly located in the cytosol and translocates to the OMM to initiate mitochondrial fission in response to stress (Ong et al., 2010).The OMM-anchored proteins mitofusin 1 and 2 (Mfn1 and Mfn2, respectively) tether the OMM together to mediate mitochondrial fusion (Ranieri et al., 2013). Optic atrophy 1 (OPA1) can be divided into an IMM-anchored long form (L-OPA1) and an IMS-distributed short form (S-OPA1). OPA1 is the key protein to induce IMM fusion and to maintain cristae structure, which is correlated to mitochondrial function (Cipolat et al., 2006). The IMM consists of two sub-compartments, i.e. the boundary membrane and the cristae, and the connection between these two sub-compartments form tubular structures that are small in diameter, known as mitochondrial crista junctions (Zick et al., 2009). Cristae are studded with proteins, including respiratory chain supercomplexes (RCSs) and ATP synthase (Mannella, 2006), which enable mitochondria to synthesize sufficient ATP to meet the energy demands of the heart. In addition to OPA1 allowing fusion, the oligomers formed by L-OPA1 and S-OPA1 tighten crista junctions, which stabilizes RCSs (to increase the efficiency of ATP production) (Cipolat et al., 2006; Cogliati et al., 2013; Frezza et al., 2006) and prevents cytochrome c release (to inhibit the initiation of apoptosis). OMA1 cleaves L-OPA1 at its S1 site to produce redundant S-OPA1 in response to stress. This breaks down the optimal ratio between L-OPA1 and S-OPA1 and leads to deterioration of cardiac function and promotion of cardiac injury (Varanita et al., 2015; Yu et al., 2016). Since excessive cleavage of OPA1 by OMA1 is closely associated with the destruction of cristae structure and mitochondrial malfunction, OMA1 inhibitors need to be found to treat patients with heart disease.

In mammalian cells, OMA1 is first translated into a precursor form that is proteolytically cleaved upon its import into mitochondria, yielding mature (M-OMA1) and lacking the N-terminal amino acid sequence 1–139 (Baker et al., 2014). Previous studies have indicated that OMA1 processing, i.e. self-cleavage of M-OMA1 and accumulation of a short form (S-OMA1) accounts for its enhanced activity towards OPA1 cleavage in response to adverse stimuli (Baker

[1]Department of Cardiology, The Second Affiliated Hospital and Yuying Children's Hospital of Wenzhou Medical University, Wenzhou, 325000, Zhejiang Province, China. [2]Cardiovascular Key Laboratory of Zhejiang Province, Department of Cardiology The Second Affiliated Hospital Zhejiang University School of Medicine, Hangzhou, 310009, Zhejiang Province, China. [3]Department of Urology, The Second Affiliated Hospital and Yuying Children's Hospital of Wenzhou Medical University, Wenzhou, 325000, Zhejiang Province, China. [4]Shanghai University of Traditional Chinese Medicine, Shanghai, 201203, China. [5]Clinical Research Center, The Second Affiliated Hospital Zhejiang University School of Medicine, Hangzhou, 310009, Zhejiang Province, China.
*These authors contributed equally to this work

‡Authors for correspondence (huangmingyuan88@163.com; fiasanar@gmail.com)

C.N., 0000-0001-6771-1761; L.Q., 0000-0001-6025-3665; Y.G., 0000-0002-1340-5715; D.X., 0000-0002-1176-4191; M.S.U.R., 0000-0001-7010-724X; M.H., 0000-0003-2149-652X

Received 31 May 2018; Accepted 27 November 2018

Journal of Cell Science (2019) 132, jcs220871. doi:10.1242/jcs.220871

et al., 2014; Zhang et al., 2014), producing redundant S-OPA1 to interfere with cristae structure and to promote cytochrome c release. Therefore, chemical compounds that inhibit OMA1 processing need to be found and their therapeutic effects tested. OMA1 has a role in both physiological and pathological situations, and fine-tunes mitochondrial bioenergetic function and respiratory supercomplex stability (Bohovych et al., 2015). Loss of this mitochondrial protease alters the cleavage pattern of OPA1, and causes obesity and defective thermogenesis in mice (Quirós et al., 2012).

In our study, 2295 plant-derived compounds were used to dock with active sites in mature OMA1 by using Molecular Operating Environment (MOE) software. According to the ranking score resulting from the docking simulation and drug-likeness analysis, epigallocatechin gallate (EGCG) and betanin were potential compounds to inhibit self-cleavage of OMA1. *In vitro* studies were also conducted to validate the inhibitory efficiency of EGCG and betanin on OMA1. We confirmed that EGCG but not betanin inhibited self-cleavage of OMA1 to reduce the proteolytic process of OPA1 upon hypoxia-reperfusion injury (HRI) and subjection to H_2O_2, eventually alleviating the deterioration of cristae structure and ensuing cytochrome c release to protect cardiomyocytes from apoptosis.

RESULTS

Self-cleavage of OMA1 correlates with OPA1 cleavage to initiate apoptosis in MEFs during HRI

Lack of OMA1 protects the kidney against IRI, suggesting that OMA1 contributes to IRI (Xiao et al., 2014). Induction of mitochondrial depolarization, by subjecting MEFs to H_2O_2 (Baker et al., 2014) or HeLa cells to the inhibitor of oxidative phosphorylation CCCP (Zhang et al., 2014), promotes self-cleavage of OMA1 (OMA1 activation) and subsequently, induces OPA1 cleavage and morphological abnormality of mitochondria (Baker et al., 2014; Zhang et al., 2014). In cardiomyocytes, IRI is associated with H_2O_2 production (Slezak et al., 1995) and mitochondrial depolarization (Sack, 2006). We speculate that IRI induces OMA1 activation and ensues OPA1 cleavage in cardiomyocytes. To simulate IRI *in vivo*, we subjected MEFs *in vitro* to HRI in our study. To verify that self-cleavage of OMA1 induces OPA1 cleavage to initiate apoptosis in MEFs upon HRI, we knocked down endogenous OMA1 in MEFs and ectopically expressed wild-type OMA1, as well as OMA1 (E324Q) – in which Glu324 had been replaced with Gln in order to maintain its non-activated status. We observed that HRI can induce the accumulation S-OMA1 (Fig. 1A) and S-OPA1 (Fig. 1B, bands c and e), whereas M-OMA1 (Fig. 1A) and L-OPA1 (Fig. 1B, bands a,b) disappeared. By contrast, in OMA1 (E324Q)-expressing MEFs, HRI failed to induce the self-cleavage of OMA1 (Fig. 1A); moreover, OPA1 was also preserved (Fig. 1B, bands a,b). These data indicate that HRI accounted for self-cleavage dependent activation of OMA1, which subsequently induced the cleavage of OPA1 protein bands a and b into protein bands c and e. A previous study has proven that OPA1 is crucial for the formation of crista junctions and the inhibition of cytochrome c release under stress conditions (Cipolat et al., 2006). In our current study, cytochrome c release was significantly decreased in OMA1 (E324Q)-expressing MEFs compared with OMA1-expressing MEFs upon HRI (Fig. 1C), suggesting that OMA1-activation-dependent cleavage of OPA1 promotes cytochrome c release. Accordingly, active-caspase3 were significantly decreased in OMA1 (E324Q)-expressing MEFs when compared with OMA1-expressing MEFs upon HRI (Fig. 1D). Taken together, the results of these experiments strongly supported our hypothesis that self-cleavage of OMA1 correlates with OPA1 cleavage to initiate apoptosis in MEFs upon HRI.

In silico docking and simulation reveals that EGCG and betanin are candidate inhibitors of OMA1

In mitochondria, OMA1 exists as a mature form that lacks 139 N-terminal amino acids (Fig. 2A) (Baker et al., 2014). In response to oxidative stress, activity of OMA1 is significantly enhanced by

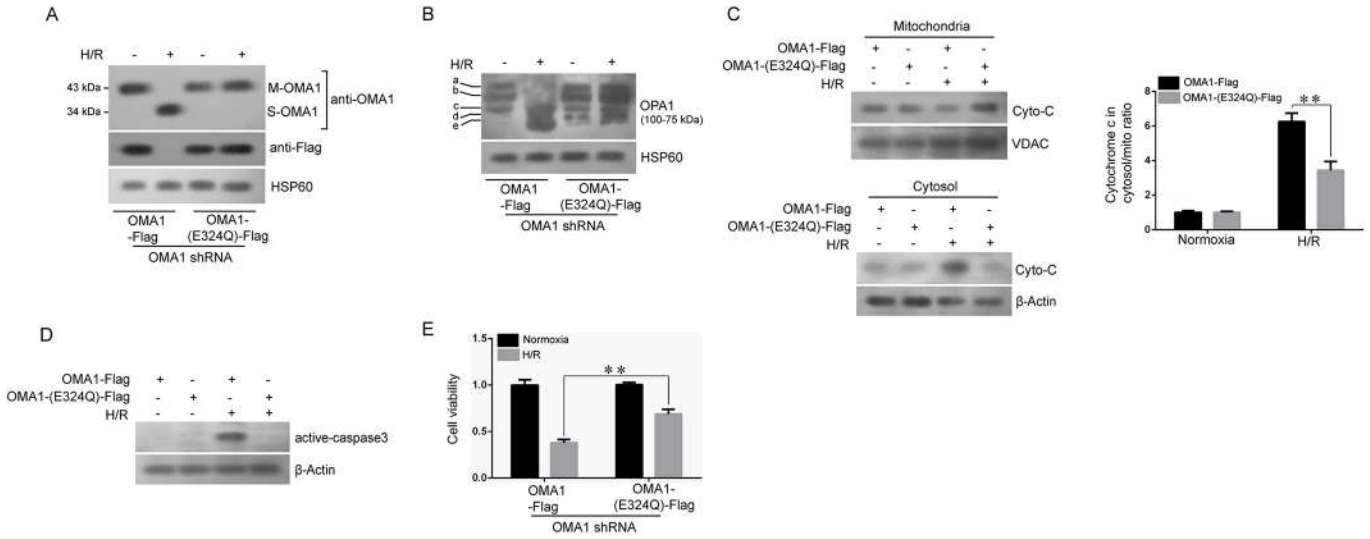

Fig. 1. Self-cleavage of OMA1 correlates with OPA1 cleavage to initiate apoptosis in MEFs during HRI. (A) MEFs were first transfected with OMA1-shRNA to knock down endogenous OMA1. Adenoviruses containing wild-type OMA1 or OMA1 (E324Q) were simultaneously transfected into the cells, which were then incubated under either normoxic conditions or subjected to HRI. Western blotting was performed using an antibody against OMA1 and FLAG. HSP60 served as loading control. (B) Western blotting was performed using an antibody against OPA1 in cells treated as described in A. Labels a–e correspond to OPA1 of different sizes; i.e. bands a and b correspond to L-OPA1, whereas bands c–e correspond to S-OPA1. (C) Western blotting was performed using an antibody against cytochrome c (Cyto-C) using cells treated as described in A. VDAC and β-actin served as a loading control for mitochondria and cytosol, respectively. Bar graph shows the change of the cytoplasmic to mitochondrial ratio of cytochrome c. (D) Western blotting was performed using an antibody against active-caspase3 using cells treated as described in A. (E) MTT assay was employed to detect cell viability of cells treated as described in A.

Journal of Cell Science (2019) 132, jcs220871. doi:10.1242/jcs.220871

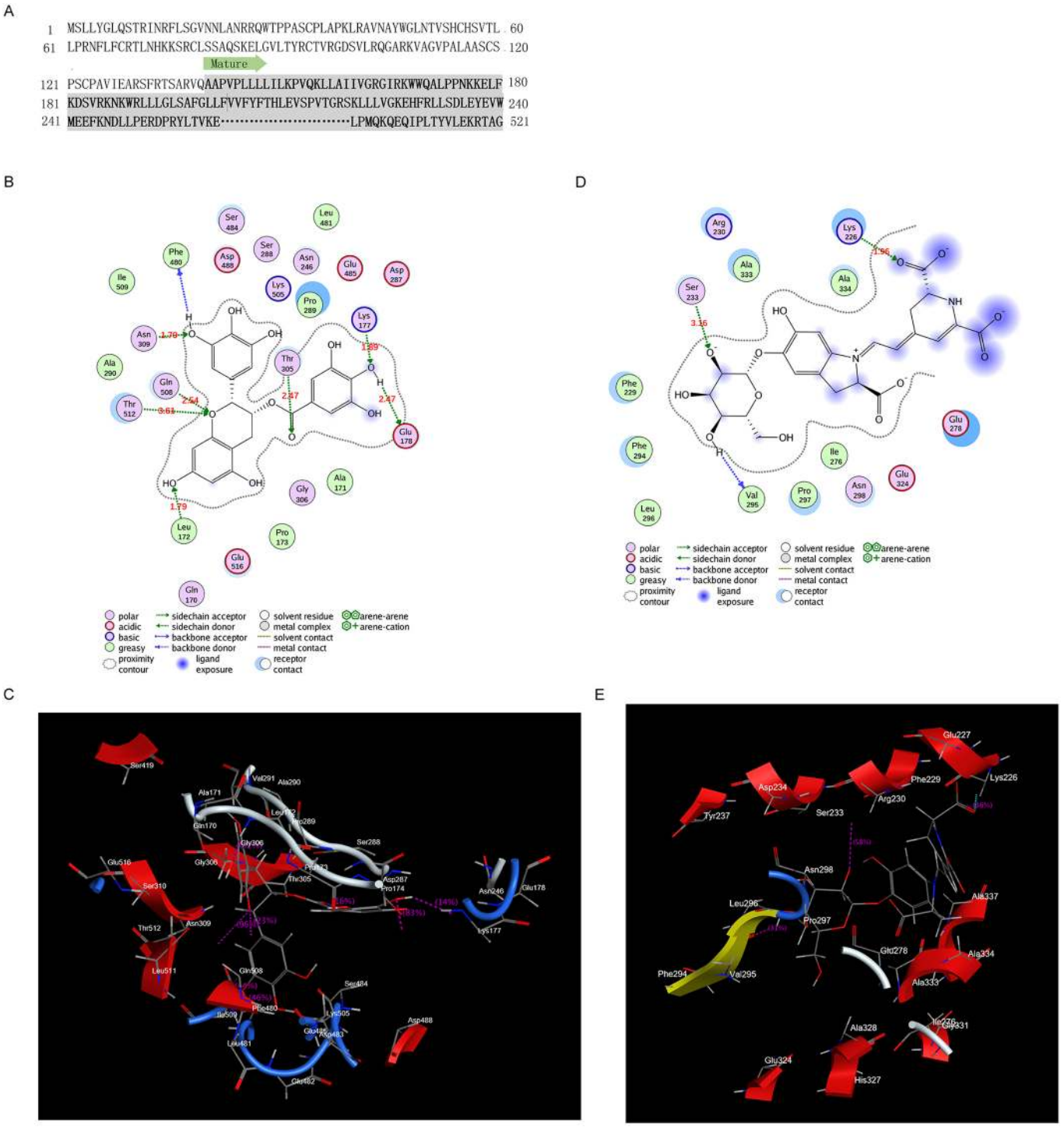

Fig. 2. *In silico* docking and simulation reveal that EGCG and betanin are candidate inhibitors of OMA1. (A) M-OMA1 is generated upon proteolytic cleavage at the site indicated by an arrow. The M-OMA1 sequence ranges from N-terminal A140 to G521, the last amino acid at C-terminal (gray background). (B,D) Docking simulation between compounds and M-OMA1 were employed using MOE software, which provided 2D diagrams for the complex between EGCG and OMA1 (B), and between betanin and OMA1 (D). The chemical structures of EGCG and betanin are shown in the center (B and D, respectively), with the key interacting amino acids shown around each. Annotations of atom properties and interaction patterns are shown below. The proximity contour indicates the space available for substitutions on the ligand. Blue regions plotted onto the atoms indicate the solvent-accessible surface area of the ligand. Arrows with dotted lines indicate hydrogen bonds. (C,E) 3D models of the docking conformation between EGCG and M-OMA1 (C), and betanin and M-OMA1 (E).

OMA1 processing (self-cleavage of M-OMA1 and accumulation of S-OMA1), which subsequently induces OPA1 cleavage and, eventually, leads to mitochondrial fragmentation, cytochrome c release and apoptosis (Zhang et al., 2014). Therefore, to protect cells from oxidative stress, the candidate inhibitors should be found to block the self-cleavage of M-OMA1. To screen for potential plant-based inhibitors of mature OMA1, we used our own small-molecule database of plant-derived inhibitors. MOE software was employed to screen for docking between mature OMA1 and its inhibitors, which we then validated by using cell models, such as MEFs and NMCMs.

Journal of Cell Science (2019) 132, jcs220871. doi:10.1242/jcs.220871

Assisted by the research group of Yang Zhang (University of Michigan, Medical School, Ann Arbour, MI), we used amino acids 140–521 of OMA1 to construct the 3-dimensional (3D) structure of mature OMA1. Simultaneously, after uploading the compound information to MOE, a compound library was established to ensuing docking in the MOE system. As discussed in the Materials and Methods, we confirmed active sites within the structure of mature OMA1 that should be targeted by the compounds. After the docking simulations between the 2295 plant compounds and active sites in mature OMA1, eight candidate compounds, including EGCG, betanin, malvidin, cineroside, ginkgetin, chicoric acid, carnosic acid and baicalin, were selected according the results (i.e. high or low scores) of the second rescoring stage (Table S1). Lower scores indicate more forms of interaction that are favored in binding. As an OMA1 inhibitor, the compound selected should be able to inhibit protease and metabolic enzymes. Therefore, we predicted the drug-likeness for these eight compounds. The Molinspiration software tool (http://www.molinspiration.com/) was used to find out more about the molecular properties and bioactivities of the compounds. The Molinspiration tool calculated the drug-likeness score towards GPCR ligands, ion channel modulators, kinase inhibitors, nuclear receptor ligands, protease inhibitors and enzyme inhibitors. Higher scores indicate higher bioactivity probability of a particular compound (Table S2). Scores of being both a protease inhibitor and an enzyme inhibitor, were higher for EGCG and betanin than for other compounds, indicating that EGCG and betanin are candidate inhibitors of OMA1. When evaluating cineroside, chicoric acid, carnosic acid and baicalin, the scores for them being enzyme inhibitors were high; however, scores for them being protease inhibitors were low. These results appear to rule out that these compounds inhibit OMA1 activation.

The intermolecular interaction of EGCG and betanin upon binding to M-OMA1 was analyzed by using MOE. EGCG was predicted to interact with M-OMA1 through hydrogen bonds via the amino acid residues Leu172, Lys177, Glu178, Thr305, Asn309, Phe480, Gln508 and Thr512 (Fig. 2B), whereas betanin was predicted to interact with Lys226, Ser233 and Val295 (Fig. 2D). The spatial interaction between the compounds and residues in M-OMA1 were also analyzed in a 3D model (Fig. 2C, E). Atoms in EGCG and betanin, such as oxygen and hydrogen (indicated in the 2D models in Fig. 2B,D, and 3D models in Fig. 2C, E), act as either hydrogen-bond acceptors or hydrogen-bond donors of corresponding residues in M-OMA1. Values (in Å) for the in-between distances are given in red in Fig. 2B,D. In addition, values indicating the strength of each hydrogen bond is provided in the 3D models in purple (Fig. 2C,E). OMA1 contains a conserved M48 metallopeptidase domain (according to the PROSITE database) and depends on this domain to exert its proteolytic activity. The M48 metallopeptidase domain is, according to the primary structure of OMA1, located in the middle of OMA1. As shown in Fig. 1B,C, residues within the M48 metallopeptidase domain of OMA1 – including Asp287, Ser288, Pro289, Ala290, Thr305, Gly306 and Asn309 – form hydrophobic interaction with atoms in EGCG, while Ile276, Glu278, Phe294, Val295, Leu296, Pro297, Asn298, Glu324, Ala333 and Ala334 form hydrophobic interactions with atoms in betanin. This suggests that EGCG and betanin interfere with the proteolytic activity of M-OMA1 by interacting with the M48 metallopeptidase domain.

The short form of OMA1 accumulates and stabilizes in MEFs upon stimulation with H_2O_2

We knocked down endogenous OMA1 and ectopically overexpressed FLAG-tagged OMA1. Silencing efficiency of OMA1 was validated earlier in experiments that involved MEFs transfected with negative-control shRNA (NC shRNA) and OMA1 shRNA (Fig. 3A). In our current study, MEFs injury caused by stimulation with H_2O_2 was used to mimic reperfusion injury. Being consistent with a previous study (Mao et al., 2014), we found that stimulation with H_2O_2 promoted OMA1 processing (self-cleavage of M-OMA1 and accumulation of S-OMA1). When stimulation with H_2O_2 was prolonged, protein levels of M-OMA1 decreased in a time-dependent manner, whereas S-OMA1 protein levels increased accordingly (Fig. 3B), suggesting that M-OMA1 was cleaved to yield S-OMA over time. Four hours after stimulation with H_2O_2, M-OMA1 was barely detectable and S-OMA1 had reached stable protein levels (Fig. 3B).

To verify that ectopically expressed OMA1 reflects the true physiology of OMA1, and also that accumulation of S-OMA1 is not an artifact of the ectopically expressed system, we detected the autocatalytic process of endogenous OMA1 in MEFs. We found that S-OMA1 accumulated in MEFs upon stimulation with H_2O_2 for 4 h (Fig. 3D), suggesting that the autocatalytic process of endogenous OMA1 is consistent with ectopically expressed OMA1. Levels of S-OMA1 were easily detected, whereas those of M-OMA1 could not be detected at all. To check whether the S-OMA1 form had been stabilized, we measured levels of S-OMA1 in response to stimulation with H_2O_2 after 4 h. Considering that the cell viability was not further decreased at 6 h in response to stimulation with H_2O_2 when compared with cell viability at 4 h (Fig. 3C), we employed western blotting to detect S-OMA1 at 6 h and found that S-OMA1 was still detectable, whereas M-OMA1 could hardly been detected (Fig. 3D). Taken together, these data demonstrate that S-OMA1 accumulated and stabilized in MEFs under conditions of stress.

EGCG alleviates mitochondrial fragmentation through inhibition of OMA1 and/or OPA1 signaling upon stimulation with H_2O_2

EGCG and betanin were analyzed by MTT assay to determine their toxic effects on MEFs. EGCG, at concentrations between 0 and 20 µM, did not show any toxic effects on MEFs (Fig. 4A). The safety of betanin was also determined after administrating MEFs with increasing concentrations of betanin (from 0–40 µM) followed by MTT detection (Fig. 4B). These results supported that EGCG and betanin can be employed to treat cells without cytotoxicity. Previous studies have indicated that OMA1 processing (self-cleavage of M-OMA1 and accumulation of S-OMA1) accounts for its enhanced activity following adverse stimuli (Baker et al., 2014; Zhang et al., 2014). Therefore, we examined whether EGCG and betanin interfere with OMA1 processing. We evaluated OMA1 processing in H_2O_2-stimulated MEFs by western blotting with an antibody against OMA1. The OMA1 (E324Q)-expressing group was used as negative control. In response to stimulation with H_2O_2, OMA1 processing was diminished in MEFs pre-treated with EGCG but not betanin (Fig. 4C), suggesting that EGCG has the potential to be an OMA1 inhibitor. As a substrate of OMA1, OPA1 should be regulated in MEFs pre-treated with EGCG. Indeed, EGCG attenuates OPA1 cleavage upon stimulation with H_2O_2 (Fig. 4D). Of note, excessive cleavage of OPA1 leads to mitochondrial fission and ultimately mitochondrial fragmentation. Therefore, it was justifiable to hypothesize that EGCG-attenuated OPA1 cleavage can maintain the mitochondrial network upon stimulation with H_2O_2. After incubating with placebo or EGCG for 3 h in culture medium containing Mito Tracker Red (a chemical dye to stain mitochondria), MEFs were stimulated with H_2O_2 or not for 4 h, followed by mitochondrial network examination using immunofluorescence and

Journal of Cell Science (2019) 132, jcs220871. doi:10.1242/jcs.220871

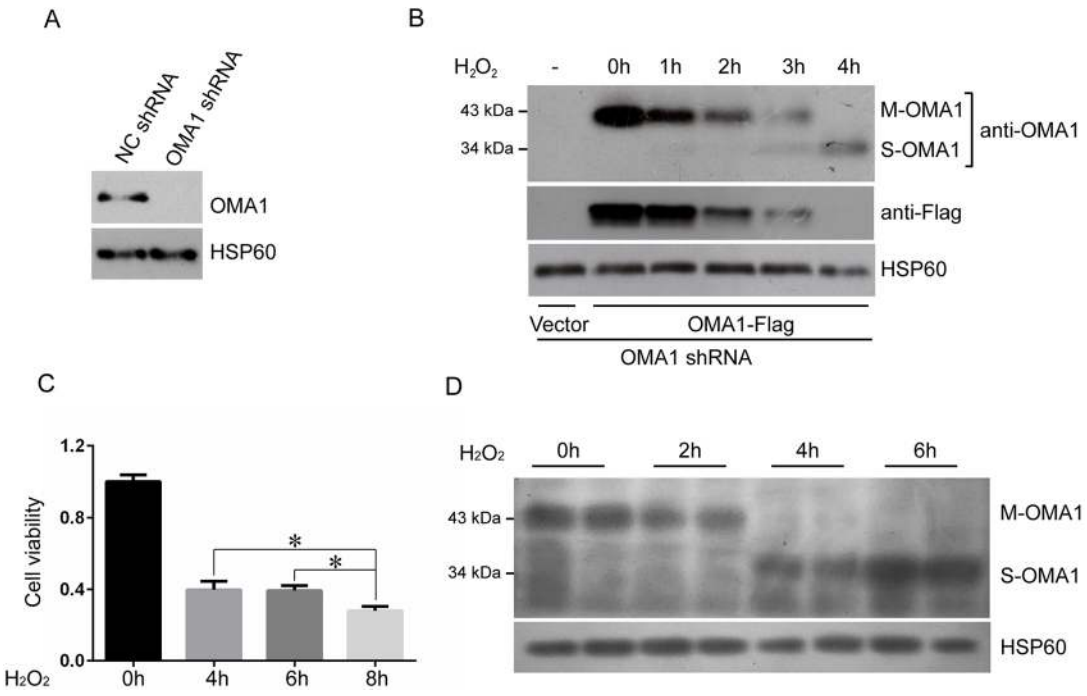

Fig. 3. Short forms of OMA1 accumulate and stabilize in MEFs upon stimulation with H_2O_2. (A) MEFs were transfected with either control-shRNA (Con-shRNA) or OMA1 shRNA for 24 h. Whole-cell extracts of MEFs were analyzed by western blotting with an antibody against OMA1. HSP60, a mitochondrial marker protein, served as loading control. (B) MEFs in which OMA1 had been knocked down by using shRNA were transfected with adenovirus expressing FLAG-tagged exogenous OMA1 for 24 h, followed by stimulation with H_2O_2 for indicated times. Western blotting was carried out to detect exogenous OMA1 using anti-OMA1 and anti-FLAG antibodies. (C) MEFs were stimulated with H_2O_2 for the indicated times, followed by MTT detection to detect cell viability. (D) MEFs were stimulated by H_2O_2 for indicated times followed by OMA1 detection by western blotting using anti-OMA1 antibody. *P<0.05.

confocal microscopy. Three major traits of mitochondrial morphology (tubular, intermediate and fragmented) were evaluated to describe mitochondrial dynamics in differently treated groups (Fig. 4E). Almost 90% of MEFs exhibited an intermediate mitochondrial morphology in the placebo- and EGCG-incubated groups even if not stimulated with H_2O_2, which made it

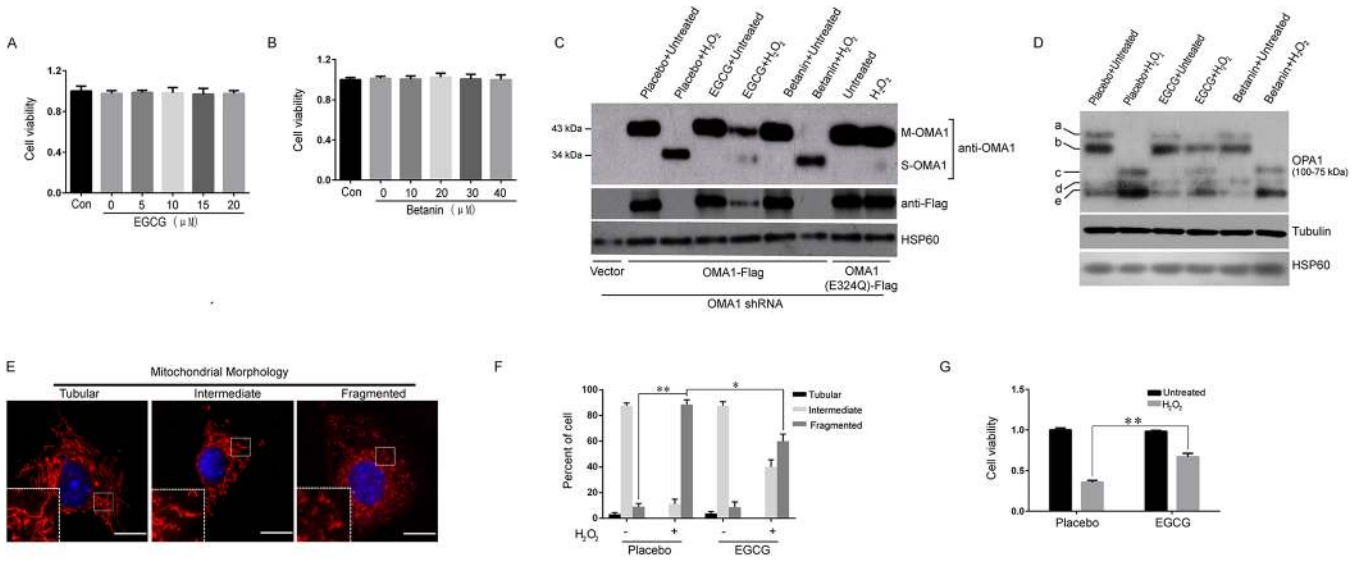

Fig. 4. EGCG alleviates mitochondrial fragmentation by inhibiting OMA1/OPA1 signaling upon stimulation with H_2O_2. (A,B) MEFs were treated with 0–20 μM EGCG (A) and 0–40 μM betanin (B) for 24 h followed by MTT detection. Con, control MEFs. (C) OMA1 knockdown MEFs were transfected to express FLAG-tagged exogenous OMA1, followed by stimulation with H_2O_2 or not, while keeping them in culture medium containing placebo, EGCG or betanin. MEFs re-expressing FLAG-tagged OMA1 (E324Q) served as negative controls, and were also stimulated or not or with H_2O_2. Western blotting was performed using anti-OMA1 and anti-FLAG antibody. (D) MEFs were incubated with placebo, EGCG or betanin for 1 h followed by stimulation with or without H_2O_2 for 4 h. Western blotting was carried out with anti-OPA1 antibody. Bands a and b indicate L-OPA1; bands c–e indicate S-OPA1 bands. (E) MitoTracker Red staining was performed on MEFs to stain the mitochondria followed by confocal microscopy examination. The representative image regarding different mitochondrial morphologies is shown. Boxed area indicates magnified area at bottom left. (F) MEFs were incubated with either placebo or EGCG for 1 h followed by stimulation with or without H_2O_2 for 4 h. The percentage of cells with different mitochondrial morphologies was calculated (n=3). (G) MEFs were treated as described in F. MTT assay was employed to detect cell viability of MEFs (n=3). **P<0.01, *P<0.05.

Journal of Cell Science (2019) 132, jcs220871. doi:10.1242/jcs.220871

hard to detect the existence of tubular and fragmented mitochondria (Fig. 4F), and suggesting that EGCG is unable to affect mitochondrial dynamics in non-stressed MEFs. Notably, MEFs that underwent stimulation with H_2O_2 showed mitochondrial fission, featuring 88% fragmented mitochondria in MEFs (Fig. 4F). With 40% intermediate and 60% fragmented mitochondria (Fig. 4F), incubation with EGCG can partially counteract the pro-fission effect of H_2O_2 on mitochondrial dynamics, which may be due to its inhibitory role in OMA1 activation and OPA1 cleavage. To assess the protective efficacy of EGCG, MTT assay was employed. It showed that cell viability of MEFs was significantly decreased following stimulation with H_2O_2 for 4 h, as compared with that of the untreated group ($P<0.01$). EGCG significantly attenuated this H_2O_2-induced decrease in cell viability ($P<0.01$) (Fig. 4G).

EGCG directly interacts with OMA1 and potently inhibits its activation to attenuate OPA1 cleavage

To fully evaluate the inhibitory capacity of EGCG on OMA1 processing, different pre-treatments were tested (Fig. 5A). We observed that, when MEFs were pre-treated with 30 µm EGCG for 2 h, EGCG reached its maximum inhibitory capacity – with OMA1 processing being completely inhibited (Fig. 5A) – indicating that EGCG is a potent OMA1 inhibitor. Accordingly, cleavage of OPA1 (i.e. cleavage of bands a and b into bands c and e, Fig. 5B), was completely inhibited when MFEs were pre-treated with 30 µm EGCG for 2 h (Fig. 5B), indicating that EGCG can affect OPA1 cleavage through inhibition of OMA1 processing. To investigate whether EGCG directly inhibits OMA1, we knocked down endogenous OMA1 and ectopically expressed wild-type OMA1 and mutant OMA1 (OMA1-L172A/K177A), i.e. L172 and K177 in OMA1 were replaced by A to abolish the interaction between EGCG and OMA1. EGCG inhibited the conversion of M-OMA1 into S-OMA1 within wild-type OMA1-expressing MEFs, which is not observed in OMA1 (L172A/K177A)-expressing MEFs (Fig. 5C). Accordingly, EGCG was unable to attenuate OPA1 cleavage in MEFs expressing OMA1 (L172A/K177A) (Fig. 5D). These data demonstrate that EGCG directly inhibits the catalytic activity of OMA1.

EGCG specifically attenuates OPA1 cleavage and maintains mitochondrial function in NMCMs during HRI

The data from our experiments using MEFs indicate that EGCG inhibits activation of OMA1, which subsequently attenuates OPA1 cleavage. To explore the potential therapeutic use of EGCG in cardiac disease, neonatal mouse cardiomyocytes (NMCMs) challenged with HRI were used to mimic IRI. As shown in Fig. 6A, EGCG did not interfere with the physiological ratio

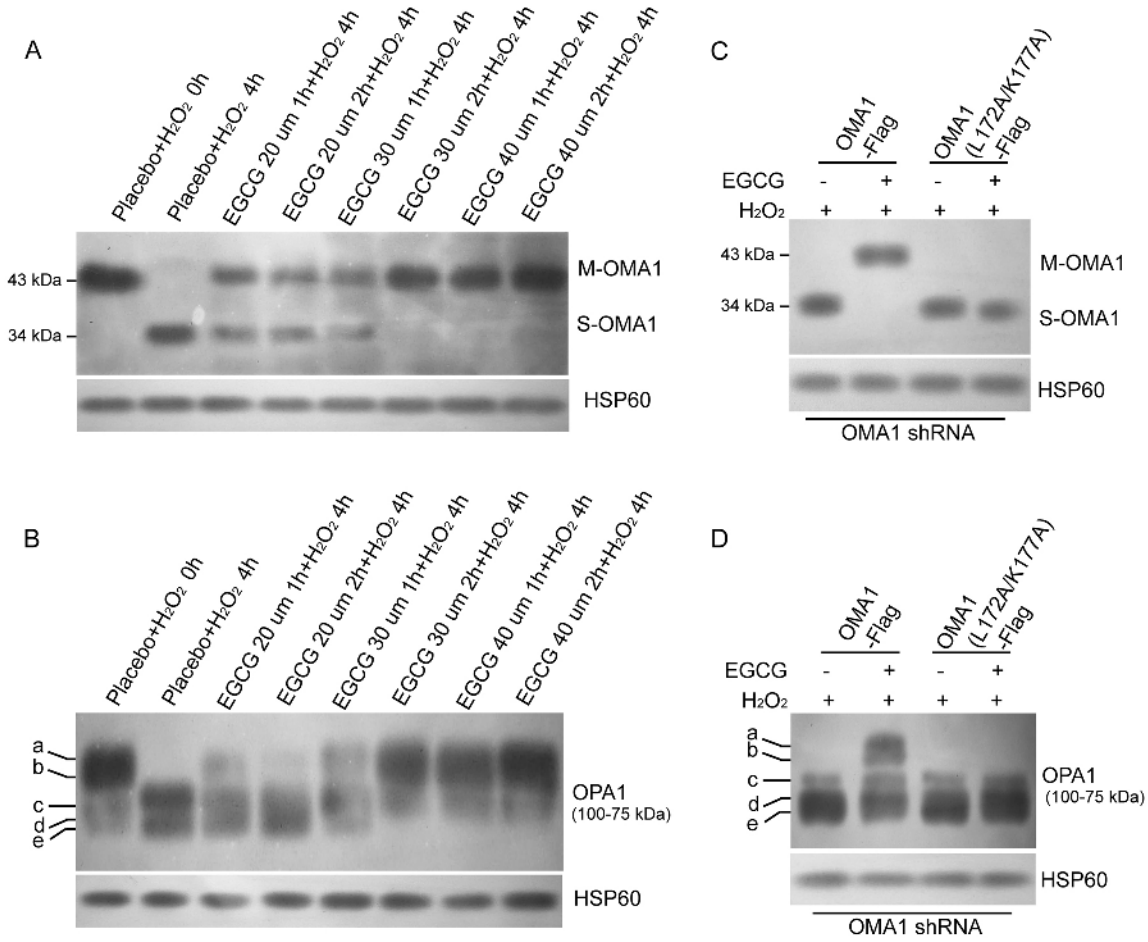

Fig. 5. EGCG directly interacts with OMA1 and potently inhibits its activation to attenuate OPA1 cleavage. (A,B) Different conditions of EGCG pre-treatment of MEFs were tested. Western blotting was carried out with anti-OMA1 (A) or anti-OPA1 (B) antibody. Bands a and b indicate L-OPA1 bands; bands c–e indicate S-OPA1 bands. (C,D) MEFs were first transfected with OMA1-shRNA to knock down endogenous OMA1. Adenovirus expressing OMA1, OMA1 with an L172A or with an K177A mutation was transfected into the cells, which were then treated with either placebo or EGCG (20 µm) for 2 h and with H_2O_2 for 4h. Western blotting was carried out with anti-OMA1 (C) and anti-OPA1 (D) antibody, respectively. HSP60 served as loading control.

Journal of Cell Science (2019) 132, jcs220871. doi:10.1242/jcs.220871

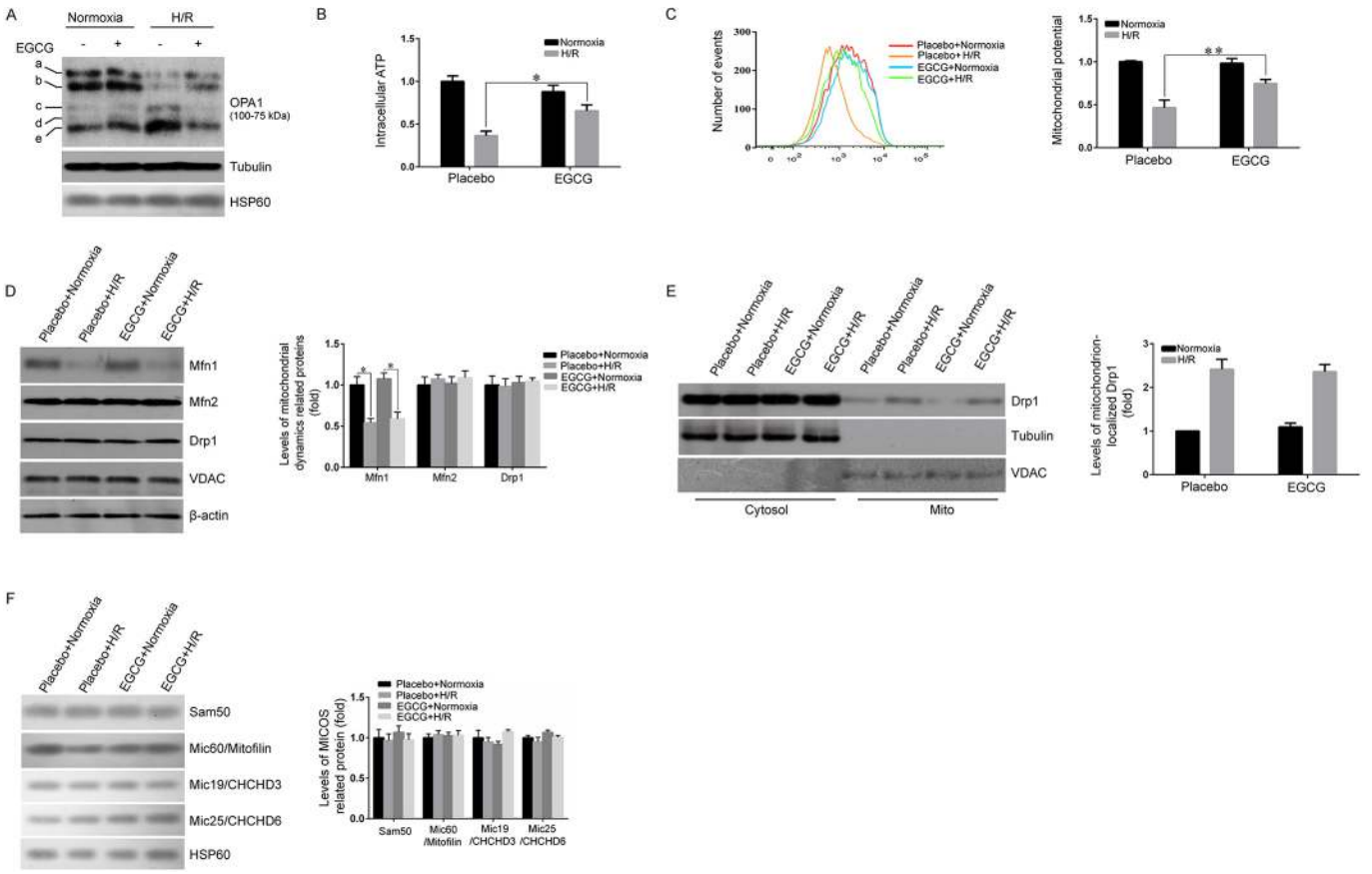

Fig. 6. EGCG specifically attenuates OPA1 cleavage and maintains mitochondrial function in mouse NMCMs during HRI. Flow cytometry was more accurate in H9C2 cells compared with NMCMs. All other experiments for which results are shown in this figure were performed by using NMCMs. (A) NMCMs were incubated with either placebo or EGCG for 1 h followed by incubation under normoxic conditions or by HRI. Western blotting was carried out to determine the cleavage of OPA1 in NMCMs. Bands a and b indicate L-OPA1 bands; bands c–e indicate S-OPA1 bands. (B) Intracellular ATP levels were determined in luciferin-/luciferase-based assays using NMCMs treated as described in A (*n*=3). (C) Mitochondrial membrane potential ($\Delta\psi$m) was measured by flow cytometric assay using H9C2 cells treated as described in A (right panel); the intensities of fluorescence regarding $\Delta\psi$m are shown in the bar graph on the left (*n*=3). (D) Whole-cell extracts from NMCMs were treated as described in A, collected and expression of mitochondrial dynamics related proteins, including Mfn1, Mfn2 and Drp1, was detected by western blotting (left panel). The mitochondrial marker protein VDAC and β-actin served as loading control. The panel on the right shows differences in the expression of MICOS-related proteins between the groups (*n*=3). (E) Mitochondrial and cytosolic protein extracts were prepared using NMCMs treated as described in A. The protein levels of Drp1, tubulin and VDAC in each extract were determined by western blotting (left panel). The differences in protein expression are shown in the bar graph (right panel) (*n*=3). (F) Whole-cell extracts from NMCMs treated as described in A were collected and expressions of core MICOS complex subunits MIC60, MIC25, MIC19 and Sam50 were detected by western blotting (left panel), with HSP60 serving as loading control. The differences in protein expression are shown in the bar graph (right panel) (*n*=3). $^{**}P<0.01$, $^{*}P<0.05$.

between L-OPA1 (bands a and b) and S-OPA1 (bands c–e) when cells were kept under normoxic conditions. L-OPA1 (bands a and b) was cleaved to its short form (bands c and e) (Fig. 6A) during HRI. NMCMs pre-treated with EGCG show attenuated OPA1 cleavage during HRI (Fig. 6A). L-OPA1 cleavage by OMA1 does not produce band d. OPA1 has been implicated in mitochondrial dynamics, which correlate with improved mitochondrial function (Cogliati et al., 2013). As expected, when compared with the placebo-treated group, the EGCG-treated group exhibited much-improved ATP production ($P<0.05$) and mitochondrial potential ($P<0.01$) during HRI (Fig. 6B, C).

Mitochondrial dynamics have been implicated in mitochondrial function, including producing ATP and maintaining mitochondrial potential (Wai and Langer, 2016). OPA1 is one of the core proteins regulating mitochondrial dynamics (Nan et al., 2017). To determine whether EGCG regulates mitochondrial dynamics specifically via OMA1/OPA1 signaling during HRI, protein levels and sub-cellular distribution of other mitochondrial dynamics related proteins (including Mfn1, Mfn2 and Drp1) were evaluated by western blotting. In NMCMs pre-treated with placebo and EGCG, protein expressions of Mfn1 were decreased to the same extent during HRI (Fig. 6D). Total protein levels of Mfn2 and Drp1 did not change significantly in each group (Fig. 6D). When evaluating the sub-cellular distribution of Drp1, we found that, during HRI, translocation of Drp1 from cytosol to mitochondria was increased, and this process cannot be affected when adding EGCG (Fig. 6E). This detection of mitochondrial dynamics-related proteins demonstrated that EGCG solely depends OMA1/OPA1 signaling to regulate mitochondrial dynamics and mitochondrial function.

In addition to OPA1, the mitochondrial contact site and cristae organizing system (MICOS) is also central in the maintenance of the cristae structure and it is located in the mitochondrial inner membrane (Kozjak-Pavlovic, 2017). MICOS is also crucial for the regulation of mitochondrial function (Genin et al., 2018). Four core components of MICOS, including the MICOS complex subunits MIC60, MIC25 and MIC19 (officially known as IMMT, CHCHD6 and CHCHD3, respectively), and the sorting and assembly machinery component 50 homolog (Samm50), were evaluated by

Journal of Cell Science (2019) 132, jcs220871. doi:10.1242/jcs.220871

western blotting (Fig. 6F). The total protein levels regarding the core components of MICOS did not change significantly in each group (Fig. 6F). From the perspective of protein expression, EGCG does not affect assembly and function of MICOS and solely depends on OMA1/OPA1 signaling to regulate cristae structure.

EGCG maintains mitochondrial morphology and cristae structure to alleviate the initiation of apoptosis in cardiomyocytes

The correct ratio between L-OPA1 and S-OPA1 is a prerequisite to tighten crista junctions. As shown in Fig. 1B, OPA1 was cleaved from long form to short form during HRI. And EGCG was able to inhibit OMA1 and attenuate OPA1 cleavage (Fig. 1A,B). Therefore, we inferred that EGCG is able to keep a relatively normal cristae structure to resist HRI challenge in NMCMs. To verify this hypothesis, NMCMs were pre-treated with either placebo or EGCG and cultured under normoxic conditions or HRI. Afterwards, NMCMs were harvested to detect cellular apoptosis and the structure of cristae. As shown in Fig. 7A, NMCMs cultured under normoxic conditions showed tightly arrayed cristae structure. Following reperfusion injury, destruction of cristae and vacuole formation were observed in mitochondria. EGCG incubation noticeably improved cristae structure, with fewer and smaller vacuoles in mitochondria (Fig. 7A). Intact and tightened cristae can hold cytochrome c in IMS and prevent cytochrome c release in response to stress. EGCG may alleviate cytochrome c release through inhibition of OMA1/OPA1 signaling. As shown in Fig. 7B, following reperfusion injury, cytochrome c levels were increased in the cytosol and decreased in mitochondria, suggesting that cytochrome c is released from mitochondria to cytosol in both placeboes and EGCG pre-treated NMCMs (Fig. 7B). However, when compared with the placebo pre-treated group, cytochrome c release was significantly alleviated in EGCG pre-treated group during HRI (P<0.01). The release of cytochrome c can, ultimately, cause the activation of caspase-3. We observed that protein levels of active caspase-3 (Fig. 7C) and TUNEL-positive nuclei (Fig. 7D) (P<0.05) were correlated with the release of cytochrome c, suggesting that EGCG can significantly attenuate activation of caspase-3 and apoptosis. Furthermore, the morphometric analysis of mitochondria and cristae were evaluated in the *in vivo* study. A total of 12, 8-week-old male mice, including six mice fed with EGCG and six mice fed with placebo were used. Each group of mice fed with EGCG or placebo was randomly assigned to either the sham (n=3) or HRI group (n=3), and mitochondrial morphology and cristae structure were established by using transmission electron microscopy (TEM). TEM showed that sham-operated mice in both placebo- and EGCG-fed groups displayed round and rectangular mitochondria, i.e. mitochondria near the cell membrane are mainly round, wheras those between muscle filaments are mainly rectangular – displaying the mitochondrial morphology of normal mouse cardiomyocytes. (Fig. 7E). Compared with sham-operated mice, HRI mice in the

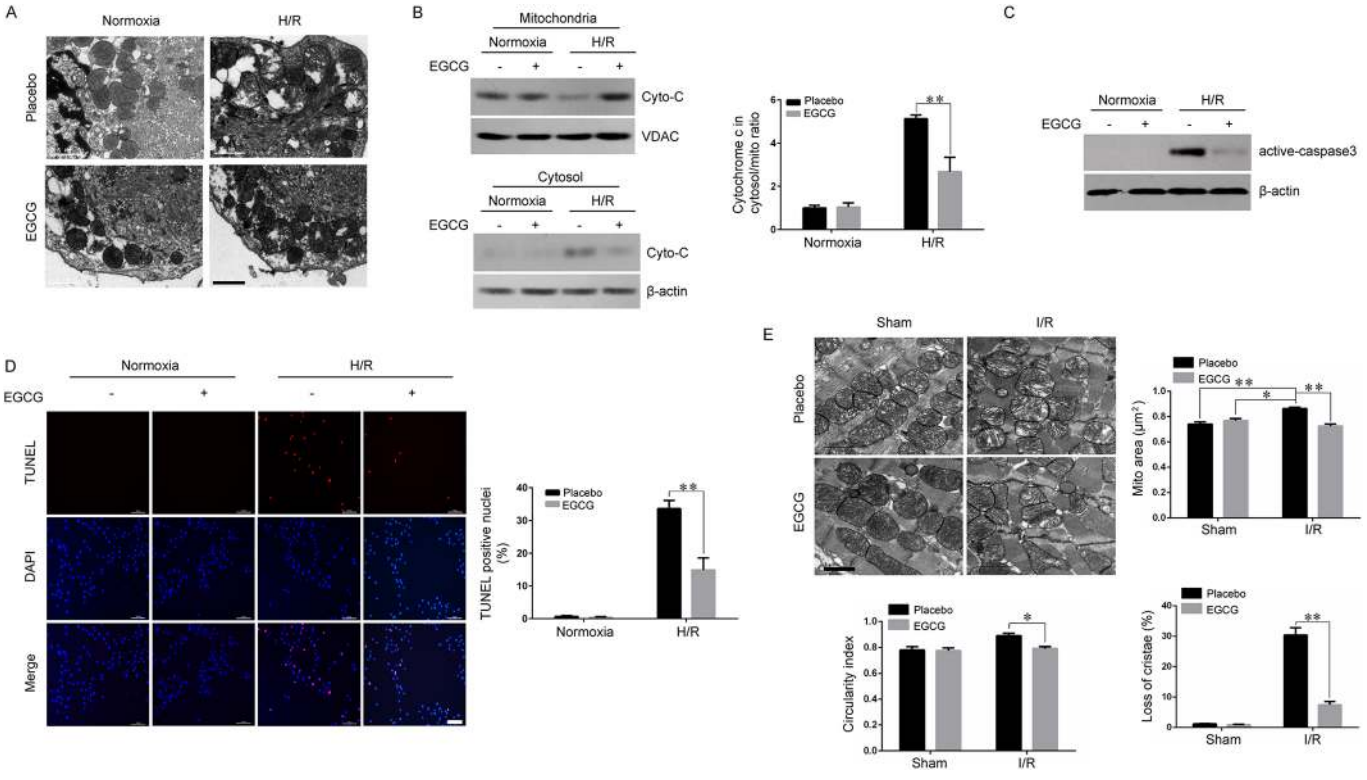

Fig. 7. EGCG maintains mitochondrial morphology and cristae structure to alleviate the initiation of apoptosis in mouse cardiomyocytes. (A) NMCMs were pre-treated with either placebo or EGCG, followed by TEM examination after normoxia incubation or HRI. Representative images are shown (scale bars: 0.5 µm). (B) Mitochondrial and cytosolic extracts of NMCMs in each group were collected. In each extract, protein levels of cytochrome c (Cyto-C) were detected by western blotting (left). VDAC; β-actin served as loading control. The bar graph on the right shows the change of the cytoplasmic to mitochondrial ratio of cytochrome c. (C) Whole-cell extracts of NMCMs in each group were collected, followed by western blotting using an antibody against active-caspase-3. (D) Representative images of TUNEL-positive NMCMs (left panel, scale bar: 100 µm). The percentage of TUNEL-positive nuclei in NMCMs was calculated for each group and the data are shown in the bar graph (right). (E) Mice were fed either placebo or EGCG, followed by sham-treatment or subjection to HRI and were then collected for TEM examination. Representative images are shown in the top left panel (scale bars: 1 µm). Average mitochondrial area (in µm^2), circularity index and loss of cristae (in %) were calculated using TEM analysis (n=3, 100 mitochondria per group). *P<0.05, **P<0.01.

Journal of Cell Science (2019) 132, jcs220871. doi:10.1242/jcs.220871

placebo-fed group displayed significantly increased swelling of mitochondria (established by measuring the circularity index and the mitochondrial area) and significantly increased vacuole formation (established by measuring the loss of cristae) (Fig. 7E) ($P<0.05$). These changes, including swelling of mitochondria and vacuole formation, were significantly attenuated in the EGCG-fed group ($P<0.05$).

DISCUSSION

OMA1 processing (self-cleavage of M-OMA1 and accumulation of S-OMA1) accounts for its enhanced activity towards OPA1 cleavage following adverse stimuli (Baker et al., 2014; Zhang et al., 2014). Therefore, we simulated docking between mature OMA1 and 2295 plant-derived compounds by using the MOE system, searching for potential inhibitors that interfere with the autocatalytic process of M-OMA1. Based on the s-score values, eight of these compounds were found to have a higher possibility to interact with active sites on M-OMA1. On the basis of the drug-likeness score of these eight compounds, only EGCG and betanin held the promise to be inhibitors for protease and enzymes. Thereafter, *in vitro* studies were conducted to validate the inhibitory efficacy of EGCG and betanin against the autocatalytic process of M-OMA1. MEFs and NMCMs were subjected to H_2O_2 and/or HRI, and these two cell models were used to mimic oxidative stress during cardiac IRI in humans. When MEFs were subjected to H_2O_2 and HRI, M-OMA1 underwent self-cleavage and S-OMA1 accumulated, and this process was correlated OPA1 cleavage (L-OPA1 was cleaved into S-OPA1). OMA1 processing was potently blocked by administration of EGCG and accompanied with attenuated OPA1 cleavage. Moreover, EGCG significantly alleviated mitochondrial dysfunction, cytochrome c release and initiation of apoptosis when NMCMs were subjected to HRI.

Reperfusion injury, including HRI and IRI, is accompanied with over-production of oxygen species (oxidative stress), leading to deterioration of homeostasis and cellular functions (Tompkins et al., 2005). Molecular events underlying oxidative stress following reperfusion injury are complex and involve loss of mitochondrial potential and ATP production, which ultimately leads to mitochondrial dysfunction and cellular apoptosis (Di Lisa and Bernardi, 2006). In our study, we observed OMA1 processing as well as OPA1 cleavage, both of which play a key role in inducing mitochondrial dysfunction and cellular apoptosis during reperfusion injury. This study demonstrated that oxidative stress depends on OMA1/OPA1 signaling to deteriorate homeostasis and function of cells following reperfusion injury.

OMA1 depends on the M48 metallopeptidase domain to exert its proteolytic activity (Baker et al., 2014). The M48 metallopeptidase domain of OMA1 cleaves L-OPA1 at the S1 site to produce S-OPA1 (Baker et al., 2014). According to the data provided by MOE, we found that EGCG was able to interact with the active site within the M48 metallopeptidase domain. Since OMA1 processing accounts for its enhanced activity towards OPA1 cleavage (Zhang et al., 2014), we infer that EGCG interferes with OPA1 cleavage by using two mechanisms: (1) EGCG interacts with the active site within the M48 metallopeptidase domain to block OMA1 processing; (2) the M48 metallopeptidase domain of OMA1 interacts with and cleaves OPA1 at the S1 site, which is competitively blocked by EGCG.

EGCG, the major catechin accounting for 59% of the total catechins in green tea (Singh et al., 2011; Steinmann et al., 2013), was demonstrated to be a compound protecting mitochondrial function in response to pathological stimuli (Adikesavan et al., 2013; Devika and Stanely Mainzen Prince, 2008a, b). TEM has been used to show that mitochondria in cardiomyocytes of rats that had been treated with isoproterenol, exhibit disarrangement and smaller size of cristae; and this was attenuated when rats were pre-treated with EGCG (Devika and Stanely Mainzen Prince, 2008a). Rats exposed to cigarette smoke exhibited highly abnormal architecture of mitochondria, swelling of mitochondria, increased areas of vacuolation indicative of edema and disruption of mitochondrial cristae, whereas EGCG administrated rats that had been subjected to EGCG and cigarette smoke showed mild distortion in mitochondrial structure without swelling and normal cristae (Adikesavan et al., 2013). However, the specific underlying mechanism that relate to abnormal mitochondrial structure and cristae damage was not elucidated. In addition, EGCG has been proved to be an effective inhibitor of matrix metalloproteinase-2 (MMP2) (Deb et al., 2016; El Bedoui et al., 2005; Zhen et al., 2006) and MMP9 (Lee et al., 2014; Sarkar et al., 2016), implying that EGCG serves as a metalloproteinase inhibitor. OMA1 is also a metalloproteinase and belongs to the peptidase M48 subset (Baker et al., 2014). In this study, we proved that EGCG inhibits the metalloproteinase OMA1. The data obtained in our study support the previously reported notion that EGCG plays a crucial role in the maintenance of cardiac mitochondrial structure and function; moreover, the underlying mechanism of this notion was elucidated.

In conclusion, an *in silico* drug design strategy revealed that EGCG can be an inhibitor of OMA1. OMA1 processing accounts for its enhanced activity towards OPA1 cleavage following reperfusion injury, which was inhibited by administration of EGCG. Inhibition of OMA1/OPA1 signaling is a potential approach to attenuate reperfusion injury. When cardiomyocytes were challenged with HRI, EGCG maintained mitochondrial cristae structure and function through inhibition of OMA1/OPA1 signaling, resulting in reduced cytochrome c release and decreased cellular apoptosis. Taken together, our data support the notion that mitochondrial integrity is the key for EGCG-induced cardiac protection, thereby providing support for EGCG as a possible therapeutic agent intended to prevent and/or limit IRI in the heart.

MATERIALS AND METHODS

Antibodies and reagents

The following antibodies were used in this study: anti-OPA1 (dilution 1:2000), anti-FLAG-tag (dilution 1:1000), anti-Mfn1 (dilution 1:1000), anti-Tom20 (dilution 1:1000) and anti-active caspase3 (dilution 1:500) were from Abcam (Cambridge, MA); anti-HSP60 (dilution 1:1000), anti-VDAC (dilution 1:1000), anti-Cytochrome c (dilution 1:1000), anti-Drp1 (dilution 1:1000) and anti-Mfn2 (dilution 1:1000) were from Cell Signaling Technology (Danvers, MA); anti-tubulin and anti-OMA1 (dilution 1:2500 and 1:1000, respectively), were from Santa Cruz Biotechnology (Shanghai, China); anti-β-actin (dilution 1:2500) was from KANGCHEN (Shanghai, China). Tetramethylrhodamine methyl ester (TMRM; Sigma-Aldrich, St Louis, MO) and MitoTracker Deep Red (Invitrogen, Carlsbad, CA) were used to stain the mitochondria. EGCG (Sigma-Aldrich) and betanin (Sigma-Aldrich) were used to inhibit the enzymatic activity of OMA1. Terminal deoxynucleotidyl transferase dUTP nick-end labeling (TUNEL) kit (Roche, Mannheim, Germany) and 4,6-diamidino-2-phenylindole (DAPI) (Sigma-Aldrich) were used to determine the apoptosis. 3-(4,5-dimethylthiazol-2-yl)-2,5-diphenyltetrazolium bromide (MTT) was purchased from Sigma-Aldrich Corporation to measure the cell viability.

Cells and cell culture conditions

Neonatal mouse cardiomyocytes (NMCMs) were isolated from the hearts of neonatal C57BL6 mice using collagenase II (0.05% [w/v] (Invitrogen) and trypsin (0.05% [w/v], Genom, China) digestion. The enzymatic digestion was stopped by adding newborn calf serum. NMCMs were purified

by differential adhesion to plastic on 24- or 6-well plates (Corning, Tewksbury, MA).

NMCMs, as well as rat myoblast (H9C2) cells and MEFs (because flow cytometry was more accurate in detecting H9C2 cells than NMCMs) were maintained in Dulbecco's modified Eagle's medium (DMEM; Corning, Manassas, VA) supplemented with 10% (v/v) fetal bovine serum (FBS; Life Technologies, Paisley, UK) and penicillin/streptomycin. All cells were cultured in a 5% CO_2 and 95% atmosphere at 37°C. For the experiments shown in Figs 1, 3, 4 and 5, MEFs were used. For the experiments shown in Fig. 6C, H9C2 were used. For other experiments shown in Figs 6 and 7, NMCMs were used."

An animal model of ischemia-reperfusion injury

Eight-week-old C57BL/6 mice (male) were anesthetized by injection of sodium pentobarbital (60 mg/kg, i.p.) followed by tracheal intubation aided by a rodent ventilator. By using a standard surgical approach, ischemia-reperfusion injury (IRI) was induced by 45 min of ischemia followed by 3 h of reperfusion injury. Sham surgical procedures were performed on the control group.

In silico docking simulation analysis of plant-derived compounds with mature OMA1

The molecular docking procedures were implemented using Molecular Operating Environment (MOE, Chemical Computing Group, Quebec, Canada) software. The protein structure of mature mouse-OMA1 was obtained from Yang Zhang's Research Group (University of Michigan). 2295 plant-derived compounds were used to dock with OMA1. Prior to starting the docking simulation, mature OMA1 and plant-derived compounds were prepared in which (i) hydrogen atoms were added to the structures with a standard geometry; (ii) structures were minimized using a MMFF94s force-field; (iii) structures were protonated utilizing Protonate3D; (iv) the MOE Alpha Site Finder was used for active site searches within the enzyme structure and dummy atoms were created from the obtained alpha spheres. Molecular docking is used to predict the binding mode of the ligand within the binding sites of mature OMA1. Docking score and ligand interaction between mature OMA1 and corresponding compounds were gained.

Construction and infection of recombinant virus vectors

Lentiviruses carrying shRNA against OMA1 and recombinant adenoviruses expressing shRNA-resistant OMA1 cDNA were all provided by JiKai Biotechnology (Shanghai, China). To generate OMA1-knockdown and knock-in MEFs, endogenous OMA1 was knocked down by OMA1-shRNA followed by transfection with lentiviruses expressing exogenous shRNA-resistant OMA1. For doing this, two silent nucleotide mutations (the siRNA-resistant nucleotide sequence 5′-GACGTTACTCCCTAGAAACT-T-3′ was used to replace the original nucleotide sequence 5′-GACCTTA-CTGCCTAGAAACTT-3′) were introduced into FLAG-tagged mouse wild-type (WT) OMA1 and FLAG-tagged mutant form of OMA1 for which we generated a glutamic acid (E)-to-glutamine (Q) mutation at residue 324 (E324Q). The viruses were amplified in HEK 293T cells and titrated according to the manufacturer's instruction. Adenoviruses containing empty plasmids (vectors) and lentiviruses containing non-specific shRNAs (NC shRNA, NC-shRNA) served as controls. Cardiomyocytes were infected with purified viruses at multiplicities of infection (MOI) of 50 (for adenoviruses) and 20 (for lentiviruses treated with polybrene at a final concentration of 8 µg/ml) overnight. Each viral suspension was replaced with fresh medium the day after infection and the expression of the indicated proteins was determined by western blotting.

Preparation of cell lysates, western blots

Cell lysis was conducted following corresponding treatments, then, the proteins were extracted in RIPA solution (Beyotime, Shanghai, China) supplemented with a protease inhibitor cocktail (Roche, Base, Switzerland). Mitochondria and cytoplasmic protein fractions were obtained using a Mitochondria and Cytoplasmic Protein Extraction Kit (Beyotime Biotechnology, Shanghai, China), according to the manufacturer's instructions. Protein concentrations were determined by BCA assay (Pierce, Rockford, IL). Equal amounts of protein were resolved by SDS–PAGE and then transferred onto a polyvinylidene fluoride (PVDF) membrane (Millipore, Billerica, MA). The blots were subsequently incubated with the corresponding primary antibodies overnight followed by horseradish peroxidase-conjugated secondary antibodies incubation. Immunoreactivity was visualized using a chemiluminescence ECL Western Blot System (Millipore, Boston, MA).

Simulated hypoxia and reperfusion injury *in vitro*

Cells were first cultured under anoxic conditions (6 h) and kept under normoxic conditions (18 h) to establish an *in vitro* model of simulated hypoxia and reperfusion injury (HRI). In brief, to simulate cells cultured under ischemic conditions, they were switched from maintenance medium (DMEM) to a buffer containing (in mmol/l) 137 NaCl, 12 KCl, 0.5 MgCl2, 0.9 CaCl2, 4 HEPES, 10 2-deoxyglucose and 20 sodium-lactate (pH 7.2), and incubated at 37°C in a cell incubator flushed with 0.5% O_2 5% CO_2 and 94.5% N_2. After challenge with simulated ischemia, cells were moved back to DMEM and kept in 5% CO_2 at 37°C to simulate reperfusion injury. Normoxic cells were cultured in DMEM and flushed with 5% CO_2 at 37°C. In Figs 4C–G and Figs 5C,D, MEFs were treated with H_2O_2 for 4h. For other figures, the duration of H_2O_2 treatment is provided in Figures and Figure legends.

Mitochondrial morphology and ΔΨ measurements

Mitochondria were labeled with MitoTracker Red (100 nmol/l). The mitochondrial phenotype of each cell was categorized as tubular, intermediate or fragmented. Mitochondria displaying morphology of puncta and rods were regarded as fragmented mitochondria. Mitochondrial integration into a network was considered as tubular mitochondria. Mitochondria exhibiting both fragmented and tubular morphology were reckoned as intermediate mitochondria. Cells were visually scored and ≥80 cells were quantified per treatment group. Confocal images were obtained with an Olympus IX81 inverted microscope. The percentage of cells with each pattern were evaluated.

Mitochondrial membrane potential (ΔΨ) was measured after loading cardiomyocytes with TMRM (200 nmol/l) for 30 min. Afterwards, cells underwent trypsinization and fluorescence was assessed by flow cytometry (excitation/emission 543/560) with a BD FACSCanto II Flow Cytometer (BD Biosciences, San Jose, CA).

ATP measurements

Cellular ATP content was measured using a luciferin/luciferase-based kit (Beyotime Biotechnology, Shanghai, China), according to the manufacturer's instructions.

Cell viability and determination of apoptosis

The cell viability was measured using MTT assays according to manufacturer's protocol. The absorbance was measured at 570 nm by Micro Plate Reader (Molecular Device, SpectraMax 250). For TUNEL analysis, NMCMs were fixed with 4% paraformaldehyde, permeabilized with 0.2% Triton X-100 and then washed twice with PBS. Nucleotide and TdT enzyme mixture was added to the cells or samples for 1 h of incubation at 37°C. The nuclei were stained with DAPI. Then, the TUNEL-positive and total nuclei were observed under a fluorescence microscope (Leica, Wetzlar, Germany).

Transmission electron microscopy

For Transmission electron microscopy (TEM), NMCMs were collected and fixed in 2% formaldehyde and 2.5% (V/V) glutaraldehyde in 0.1 M Na-cacodylate buffer (pH 7.4) for 2 h at room temperature and then incubated overnight at 4°C. The cells were then washed thrice in 0.1 M PBS for 15 min each and fixed in 1% osmium tetroxide for 1 h. Then, cells were stained, blocked with uranyl acetate, dehydrated with a graded series of ethanol solutions, cleared in propylene oxide and then embedded in epoxy resin. Thereafter, the blocks were trimmed and ultra-thin sections (120 nm) were cut, which were subsequently observed under a transmission electron microscope (H7500 TEM, Hitachi, Tokyo, Japan, http://www.hitachi.com).

Statistical analysis

All values are presented as the mean±s.e. We evaluated the significance of the differences between groups by Student's *t*-test or two-way analysis of variance. $P<0.05$ was considered statistically significant. All statistical

analyses were performed using GraphPad Prism® 5.0 (GraphPad Software, Inc., La Jolla, CA).

Acknowledgements
We thank Yang Zhang (University of Michigan, Medical School, Ann Arbour, MI) for helping us with bioinformatics analysis.

Competing interests
The authors declare no competing or financial interests.

Author contributions
Conceptualization: J.N., C.N., M.H.; Methodology: J.N., C.N., J.Y., Y.G., M.S.U.R., M.H.; Software: J.N., M.S.U.R.; Validation: J.N., C.N.; Formal analysis: J.N., C.N., L.Q., Y.G., D.X.; Investigation: J.N., J.Y., D.X., M.H.; Resources: M.H.; Data curation: L.Q., Y.G., D.X.; Writing - original draft: J.N., M.S.U.R., M.H.; Writing - review & editing: J.N., M.S.U.R., M.H.; Visualization: J.N., J.Y., L.Q., M.H.; Supervision: M.H.; Project administration: M.H.; Funding acquisition: M.H.

Funding
This work was supported by the National Natural Science Foundation of China (grant no. 81800314) for J. Nan), the Natural Science Foundation of Zhejiang Province (grant no. LY18H020010) for M. Huang) and Medical Scientific Research Foundation of Zhejiang Province, China (grant no. 2018KY526).

Supplementary information
Supplementary information available online at
http://jcs.biologists.org/lookup/doi/10.1242/jcs.220871.supplemental

References
Adikesavan, G., Vinayagam, M. M., Abdulrahman, L. A. and Chinnasamy, T. (2013). (−)-Epigallocatechin-gallate (EGCG) stabilize the mitochondrial enzymes and inhibits the apoptosis in cigarette smoke-induced myocardial dysfunction in rats. *Mol. Biol. Rep.* **40**, 6533-6545.

Baker, M. J., Lampe, P. A., Stojanovski, D., Korwitz, A., Anand, R., Tatsuta, T. and Langer, T. (2014). Stress-induced OMA1 activation and autocatalytic turnover regulate OPA1-dependent mitochondrial dynamics. *EMBO J.* **33**, 578-593.

Biala, A. K. and Kirshenbaum, L. A. (2014). The interplay between cell death signaling pathways in the heart. *Trends Cardiovasc. Med.* **24**, 325-331.

Bohovych, I., Fernandez, M. R., Rahn, J. J., Stackley, K. D., Bestman, J. E., Anandhan, A., Franco, R., Claypool, S. M., Lewis, R. E., Chan, S. S. L. et al. (2015). Metalloprotease OMA1 fine-tunes mitochondrial bioenergetic function and respiratory supercomplex stability. *Sci. Rep.* **5**, 13989.

Cipolat, S., Rudka, T., Hartmann, D., Costa, V., Serneels, L., Craessaerts, K., Metzger, K., Frezza, C., Annaert, W. and D'Adamio, L. et al. (2006). Mitochondrial rhomboid PARL regulates cytochrome c release during apoptosis via OPA1-dependent cristae remodeling. *Cell* **126**, 163-175.

Cogliati, S., Frezza, C., Soriano, M. E., Varanita, T., Quintana-Cabrera, R., Corrado, M., Cipolat, S., Costa, V., Casarin, A., Gomes, L. C. et al. (2013). Mitochondrial cristae shape determines respiratory chain supercomplexes assembly and respiratory efficiency. *Cell* **155**, 160-171.

Deb, G., Batra, S. and Limaye, A. M. (2016). Data in support of the negative influence of divalent cations on (−)-epigallocatechin-3-gallate (EGCG)-mediated inhibition of matrix metalloproteinase-2 (MMP-2). *Data Brief* **6**, 461-465.

Devika, P. T. and Stanely Mainzen Prince, P. (2008a). (−) Epigallocatechin-gallate (EGCG) prevents mitochondrial damage in isoproterenol-induced cardiac toxicity in albino Wistar rats: a transmission electron microscopic and in vitro study. *Pharmacol. Res.* **57**, 351-357.

Devika, P. T. and Stanely Mainzen Prince, P. (2008b). (−) Epigallocatechingallate protects the mitochondria against the deleterious effects of lipids, calcium and adenosine triphosphate in isoproterenol induced myocardial infarcted male Wistar rats. *J. Appl. Toxicol.* **28**, 938-944.

Di Lisa, F. and Bernardi, P. (2006). Mitochondria and ischemia–reperfusion injury of the heart: fixing a hole. *Cardiovasc. Res.* **70**, 191-199.

Dorn, G. W. (2015). Mitochondrial dynamism and heart disease: changing shape and shaping change. *EMBO Mol. Med.* **7**, 865-877.

El Bedoui, J., Oak, M.-H., Anglard, P. and Schini-Kerth, V. B. (2005). Catechins prevent vascular smooth muscle cell invasion by inhibiting MT1-MMP activity and MMP-2 expression. *Cardiovasc. Res.* **67**, 317-325.

Frezza, C., Cipolat, S., Martins de Brito, O., Micaroni, M., Beznoussenko, G. V., Rudka, T., Bartoli, D., Polishuck, R. S., Danial, N. N., De Strooper, B. et al. (2006). OPA1 controls apoptotic cristae remodeling independently from mitochondrial fusion. *Cell* **126**, 177-189.

Genin, E. C., Bannwarth, S., Lespinasse, F., Ortega-Vila, B., Fragaki, K., Itoh, K., Villa, E., Lacas-Gervais, S., Jokela, M., Auranen, M. et al. (2018). Loss of MICOS complex integrity and mitochondrial damage, but not TDP-43 mitochondrial localisation, are likely associated with severity of CHCHD10-related diseases. *Neurobiol. Dis.* **119**, 159-171.

Kozjak-Pavlovic, V. (2017). The MICOS complex of human mitochondria. *Cell Tissue Res.* **367**, 83-93.

Lee, H. S., Jun, J.-H., Jung, E.-H., Koo, B. A. and Kim, Y. S. (2014). Epigalloccatechin-3-gallate inhibits ocular neovascularization and vascular permeability in human retinal pigment epithelial and human retinal microvascular endothelial cells via suppression of MMP-9 and VEGF activation. *Molecules* **19**, 12150-12172.

Lemieux, H. and Hoppel, C. L. (2009). Mitochondria in the human heart. *J. Bioenerg. Biomembr.* **41**, 99-106.

Mannella, C. A. (2006). Structure and dynamics of the mitochondrial inner membrane cristae. *Biochim. Biophys. Acta* **1763**, 542-548.

Mao, C.-Y., Lu, H.-B., Kong, N., Li, J.-Y., Liu, M., Yang, C.-Y. and Yang, P. (2014). Levocarnitine protects H9c2 rat cardiomyocytes from H2O2-induced mitochondrial dysfunction and apoptosis. *Int. J. Med. Sci.* **11**, 1107-1115.

Nan, J., Zhu, W., Rahman, M. S., Liu, M., Li, D., Su, S., Zhang, N., Hu, X., Yu, H., Gupta, M. P. et al. (2017). Molecular regulation of mitochondrial dynamics in cardiac disease. *Biochim. Biophys. Acta Mol. Cell Res.* **1864**, 1260-1273.

Neuzil, J., Widén, C., Gellert, N., Swettenham, E., Zobalova, R., Dong, L.-F., Wang, X.-F., Lidebjer, C., Dalen, H., Headrick, J. P. et al. (2007). Mitochondria transmit apoptosis signalling in cardiomyocyte-like cells and isolated hearts exposed to experimental ischemia-reperfusion injury. *Redox Rep.* **12**, 148-162.

Ong, S.-B., Subrayan, S., Lim, S. Y., Yellon, D. M., Davidson, S. M. and Hausenloy, D. J. (2010). Inhibiting mitochondrial fission protects the heart against ischemia/reperfusion injury. *Circulation* **121**, 2012-2022.

Quirós, P. M., Ramsay, A. J., Sala, D., Fernández-Vizarra, E., Rodríguez, F., Peinado, J. R., Fernández-García, M. S., Vega, J. A., Enríquez, J. A., Zorzano, A. et al. 2012). Loss of mitochondrial protease OMA1 alters processing of the GTPase OPA1 and causes obesity and defective thermogenesis in mice. *EMBO J.* **31**, 2117-2133.

Ranieri, M., Brajkovic, S., Riboldi, G., Ronchi, D., Rizzo, F., Bresolin, N., Corti, S. and Comi, G. P. (2013). Mitochondrial fusion proteins and human diseases. *Neurol. Res. Int.* **2013**, 293893.

Sack, M. N. (2006). Mitochondrial depolarization and the role of uncoupling proteins in ischemia tolerance. *Cardiovasc. Res.* **72**, 210-219.

Sarkar, J., Nandy, S. K., Chowdhury, A., Chakraborti, T. and Chakraborti, S. (2016). Inhibition of MMP-9 by green tea catechins and prediction of their interaction by molecular docking analysis. *Biomed. Pharmacother.* **84**, 340-347.

Singh, B. N., Shankar, S. and Srivastava, R. K. (2011). Green tea catechin, epigallocatechin-3-gallate (EGCG): mechanisms, perspectives and clinical applications. *Biochem. Pharmacol.* **82**, 1807-1821.

Slezak, J., Tribulova, N., Pristacova, J., Uhrik, B., Thomas, T., Khaper, N., Kaul, N. and Singal, P. (1995). Hydrogen peroxide changes in ischemic and reperfused heart. Cytochemistry and biochemical and X-ray microanalysis. *Am. J. Pathol.* **147**, 772.

Steinmann, J., Buer, J., Pietschmann, T. and Steinmann, E. (2013). Anti-infective properties of epigallocatechin-3-gallate (EGCG), a component of green tea. *Br. J. Pharmacol.* **168**, 1059-1073.

Tompkins, A. J., Burwell, L. S., Digerness, S. B., Zaragoza, C. Holman, W. L. and Brookes, P. S. (2005). Mitochondrial dysfunction in cardiac ischemia–reperfusion injury: ROS from complex I, without inhibition. *–Biochim. Biophys. Acta.* **1762**, 223-231.

Varanita, T., Soriano, M. E., Romanello, V., Zaglia, T., Quintana-Cabrera, R., Semenzato, M., Menabò, R., Costa, V., Civiletto, G., Pesce, P. et al. (2015). The OPA1-dependent mitochondrial cristae remodeling pathway controls atrophic, apoptotic, and ischemic tissue damage. *Cell Metab.* **21**, 834-844.

Wai, T. and Langer, T. (2016). Mitochondrial dynamics and metabolic regulation. *Trends Endocrinol. Metab.* **27**, 105-117.

Xiao, X., Hu, Y., Quirós, P. M., Wei, Q., López-Otín, C. and Dong, Z. (2014). OMA1 mediates OPA1 proteolysis and mitochondrial fragmentation in experimental models of ischemic kidney injury. *Am. J. Physiol. Renal. Physiol.* **306**, F1318-F1326.

Yu, J., Wu, J., Xie, P., Maimaitili, Y., Wang, J., Xia, Z., Gao, F., Zhang, X. and Zheng, H. (2016). Sevoflurane postconditioning attenuates cardiomyocyte hypoxia/reoxygenation injury via restoring mitochondrial morphology. *PeerJ* **4**, e2659.

Zhang, K., Li, H. and Song, Z. (2014). Membrane depolarization activates the mitochondrial protease OMA1 by stimulating self-cleavage. *EMBO Rep.* **15**, 576-585.

Zhen, M. C., Huang, X. H., Wang, Q., Sun, K., Liu, Y. J., Li, W., Zhang, L. J., Cao, L. Q. and Chen, X. L. (2006). Green tea polyphenol epigallocatechin-3-gallate suppresses rat hepatic stellate cell invasion by inhibition of MMP-2 expression and its activation. *Acta Pharmacol. Sin.* **27**, 1600-1607.

Zick, M., Rabl, R. and Reichert, A. S. (2009). Cristae formation—linking ultrastructure and function of mitochondria. *Biochim. Biophys. Acta.* **1793**, 5-19.